

Electric Polarizability of Charged Kaons from Lattice QCD Four-Point Functions

Shayan Nadeem,^{a,*} Walter Wilcox^a and Frank X. Lee^b

^a*Department of Physics and Astronomy, Baylor University,
Waco, Texas 76798, USA*

^b*Physics Department, The George Washington University,
Washington, District of Columbia 20052, USA*

E-mail: shayan_nadeem1@baylor.edu, walter_wilcox@baylor.edu, fxlee@gwu.edu

We study the electric polarizability of a charged kaon from four-point functions in lattice QCD as an alternative to the background field method. Lattice four-point correlation functions are constructed from quark and gluon fields to be used in Monte Carlo simulations. The elastic form factor (charge radius) is needed in the method which can be obtained from the same four-point functions at large current separations. Preliminary results from the connected quark-line diagrams are presented.

*The 41st International Symposium on Lattice Field Theory (LATTICE2024)
28 July - 3 August 2024
Liverpool, UK*

*Speaker

1. Introduction

The study of electromagnetic polarizabilities is a long-standing pursuit in hadronic physics, and its investigation within lattice QCD presents both intriguing opportunities and considerable challenges. Traditionally, the background field method has been the go-to technique for computing polarizabilities, providing reliable results for neutral hadrons. This approach has seen widespread application in various lattice studies [1–3]. However, the situation becomes considerably more complicated when dealing with charged particles. In this case, the problem is twofold: the quenching of the external electromagnetic field and the fact that charged hadrons, when placed in an external field, will experience effects like the formation of Landau levels in a magnetic field. These challenges have limited the number of lattice QCD calculations for charged hadrons, with much of the focus remaining on neutral mesons, such as the pion.

In this work, we employ the four-point functions method—an approach that, while not new, has not received as much attention in the context of polarizabilities. Four-point correlation functions have been used to study a variety of hadronic properties [4], but their potential for extracting polarizabilities has only recently been appreciated. To our knowledge, there have been two notable attempts in the past, one using position-space methods [5] and the other in momentum space [6].

The four-point function method is ideally suited for studying charged hadrons. By directly incorporating the effects of the hadronic structure in a manner that avoids many of the pitfalls of the background field approach, this method holds promise for more precise and robust calculations. Our goal is to present a detailed study of the electric polarizability of the charged kaon, using lattice QCD four-point functions, and to compare our results with those obtained from other approaches.

2. Charged Kaon

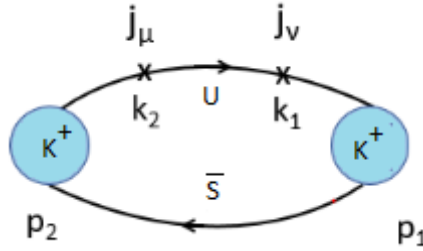


Figure 1: Pictorial representation of the four-point function in Eq.(1) for K^+ . Time flows from right to left and the four-momentum conservation is $p_2 + k_2 = k_1 + p_1$.

In Ref. [7] a formula for the electric polarizability of the charged pion is derived. For the kaon, the formula is the same except for the replacement of the pion mass with the kaon mass,

$$\alpha_E^K = \frac{\alpha \langle r_E^2 \rangle}{3m_K} + \lim_{q \rightarrow 0} \frac{2\alpha}{q^2} \int_0^\infty dt \left[Q_{44}(\mathbf{q}, t) - Q_{44}^{elas}(\mathbf{q}, t) \right]. \quad (1)$$

Here, $\alpha = 1/137$ represents the fine structure constant. The first term in the equation includes the charge radius and the kaon mass, which we will refer to as the elastic contribution. The second term

results from subtracting the elastic contribution Q_{44}^{elas} from the total, and we will call this the inelastic contribution. This formula is applied in discrete Euclidean spacetime, though we retain a continuous Euclidean time axis for ease of notation. Special kinematics, known as the zero-momentum Breit frame, are used in the formula to simulate low-energy Compton scattering. The process is illustrated in Fig. 1. Part of evaluating the four-point function is to evaluate the topologically distinct quark-line diagrams. These diagrams are shown in Fig. 2. The raw correlation functions can be found in Ref. [7].

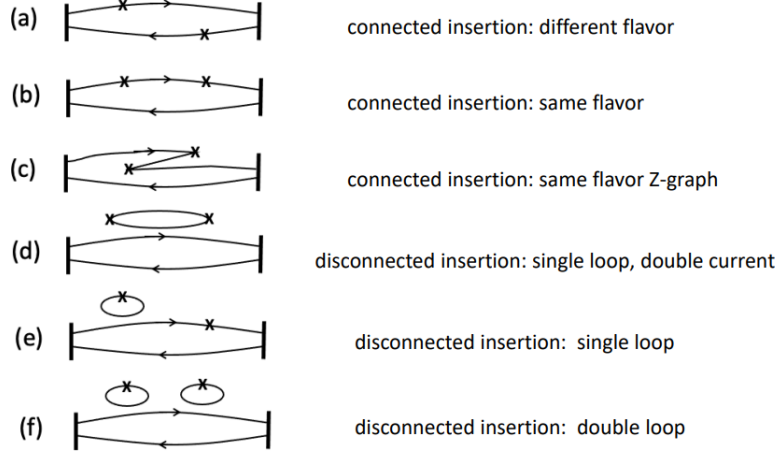


Figure 2: Skeleton diagrams of a four-point function contributing to polarizabilities of a meson: (a) connected insertion: different flavor, (b) connected insertion: same flavor, (c) connected insertion: same flavor Z-graph, (d) disconnected insertion: single loop, double current, (e) disconnected insertion: single loop, (f) disconnected insertion: double loop. In each diagram, flavor permutations are assumed as well as gluon lines that connect the quark lines. The zero-momentum pion interpolating fields are represented by vertical bars (wall sources). Time flows from right to left.

3. Simulation details and results

It is worth mentioning that our current results have some limitations. Firstly, we use 99 configurations for our analysis. This explains the comparatively large error bars. We are currently working towards performing an analysis using 500 configurations. Secondly, as a proof-of-principle simulation, we use quenched Wilson fermions.

3.1 Raw correlation functions

We present in Fig. 3 the raw normalized four-point functions Q_{44} at two different values of momentum \mathbf{q} and at $m_\pi = 600 MeV$. These plots exhibit several interesting features. First, the point where $t_1 = t_2$ behaves regularly in diagram (a) but yields irregular results in diagrams (b) and (c) for all values of \mathbf{q} . This irregularity corresponds to the contact term discussed in Ref. [7], and we exclude this point from our analysis. Second, the results around $t_1 = 18$ in diagrams (b) and (c) are mirror images of each other, which is due to the two different time orderings of the same diagram.

In principle, this symmetry could be leveraged to reduce the computational cost of simulations. However, in this study, we computed all three diagrams separately.

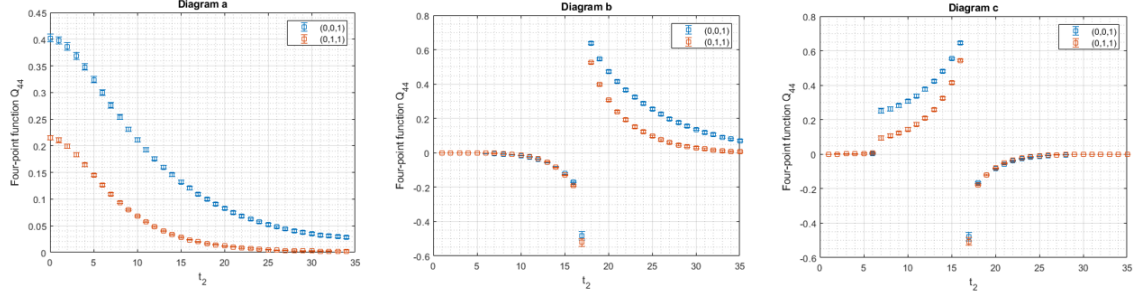


Figure 3: Normalized four-point functions from the connected diagrams as a function of current separation at $m_\pi = 600 \text{ MeV}$.

3.2 Elastic form factor

The formula for electric polarizability in Eq.(1) includes the charge radius r_E and the elastic contribution Q_{44}^{elas} , both of which can be determined from the long-time behavior of the four-point functions Q_{44} . According to the following equation given in Ref. [7],

$$Q_{44}^{elas}(\mathbf{q}, t) = \frac{(E_K + m_K)^2}{4E_K m_K} F_K^2(\mathbf{q}^2) e^{-a(E_K - m_K)t}. \quad (2)$$

Q_{44}^{elas} is expected to follow a single-exponential behavior with a decay rate of $E_K - m_K$. The form factor F_K is embedded in the amplitude of this decay. As discussed in Ref. [7], diagrams *a* and *b* display the expected decay, while diagram *c* does not. For the elastic contribution, we can omit

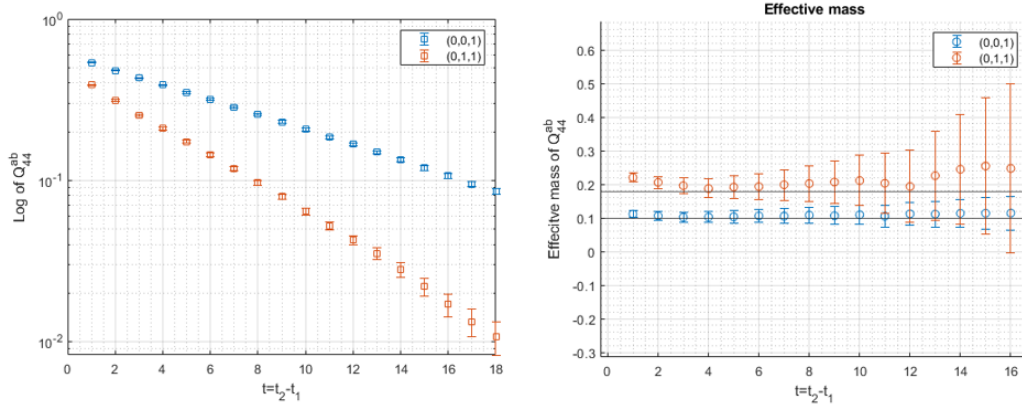


Figure 4: Normalized four-point functions from diagrams *a* and *b* in log plot and their effective mass functions at different values of \mathbf{q} and $m_\pi = 600 \text{ MeV}$. They are plotted as functions of time separation $t = t_2 - t_1$ between the two currents relative to fixed $t_1 = 18$. The horizontal gridlines in the effective mass are $E_K - m_K$ using continuum dispersion relation for E_K with measured m_K . These functions are used to extract the elastic contributions Q_{44}^{elas} .

diagram c and concentrate on diagrams a and b , which enhances the form factor analysis by removing the inelastic 'contamination' from diagram c , serving as an optimization in the analysis.

Fig. 4 provides an example of the four-point functions Q_{44}^{ab} , including only diagrams a and b , along with their effective mass functions. We focus on the signal region between t_1 and t_3 , plotting them as a function of the time separation $t = t_2 - t_1$ between the two currents. The $t = 0$ point is excluded from the analysis due to contact terms, as mentioned earlier. There is a region where the effective mass functions align with the $E_K - m_K$ gridlines, indicating that Q_{44}^{ab} is primarily governed by elastic contributions. This agreement is more pronounced at lower momentum values. At larger times, the signal becomes noisy, particularly at higher momentum.

To address potential deviations from the continuum dispersion relation, we fit the functional form of Q_{44}^{elas} in Eq.(2), treating F_K, E_K as free parameters while keeping m_K fixed at its measured value from two-point functions. After the form factor data are obtained, we fit them to the monopole form,

$$F_\pi(q^2) = \frac{1}{1 + q^2/m_V^2}, \quad (3)$$

which is the well-known vector meson dominance (VMD) commonly considered in pion form factor studies. We use the monopole form because of the availability of just two momenta. As we move on with our analysis, we will be working with data for four momenta, at which point we will be using the z -expansion parametrization [8] for a better fit. The results are illustrated in Fig. 5. Once the

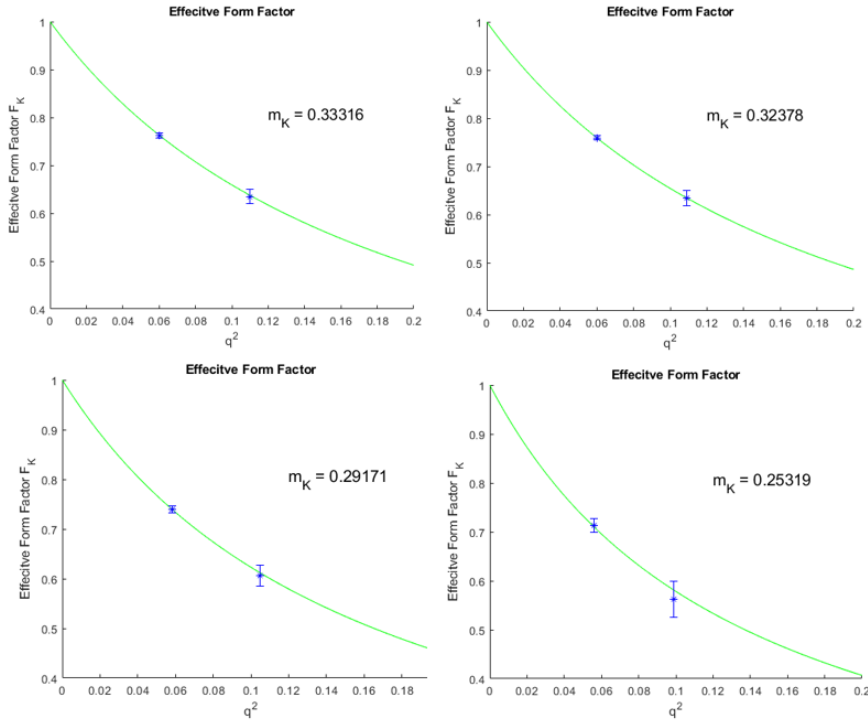


Figure 5: Pion elastic form factors extracted from four-point functions. The blue data points are the measured values. The green solid line is a fit to the monopole form in Eq. (3). m_K and q^2 values in lattice units.

functional form of form factor is determined, the charge radius is obtained by

$$\langle r_E^2 \rangle = -6 \frac{dF_K(q^2)}{dq^2} \Big|_{q^2 \rightarrow 0}. \quad (4)$$

3.3 Electric polarizability

After determining the elastic contribution Q_{44}^{elas} , we now focus on the inelastic part of α_E from Eq.(1). In Fig. 6, we present the total contribution Q_{44} (from all three diagrams) and Q_{44}^{elas} as functions of the current separation $t = t_2 - t_1$, using $m_\pi = 600$ MeV as an example. The graphs for other pion masses are similar. Although Q_{44}^{elas} is derived from the large-time region, the subtraction is applied across the entire region based on the functional form in Eq.(2). Most contributions arise from the small-time region where inelastic effects are more prominent. We observe that Q_{44}^{elas} consistently exceeds Q_{44} , implying a negative inelastic term in the formula. The time integral corresponds to the negative of the area between the two curves. Notably, the curves include the

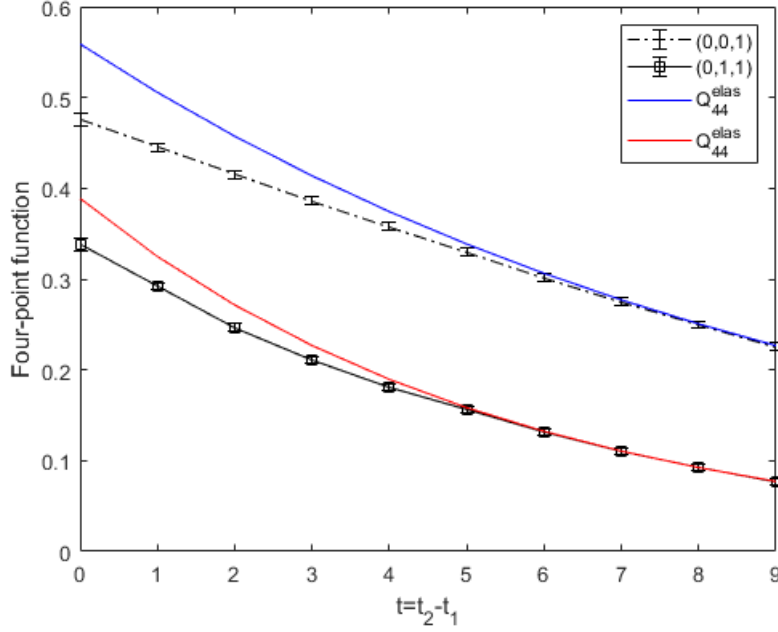


Figure 6: Total Q_{44} and elastic Q_{44}^{elas} at different values of q at $m_\pi = 600$ MeV. The area between the curves, $(1/a) \int dt [Q_{44}(q, t) - Q_{44}^{elas}(q, t)]$, is the dimensionless signal contributing to polarizability.

$t = 0$ point, which contains unphysical contributions in Q_{44} , as previously mentioned. Typically, we would exclude this point and start the integral from $t = 1$. However, the area between $t = 0$ and $t = 1$ constitutes the largest portion of the integral. To account for this, we linearly extrapolated the Q_{44} term back to $t = 0$ using the values at $t = 1$ and $t = 2$. This introduces a systematic effect of order $O(a^2)$, as the error itself is of order $O(a)$. This effect diminishes as the continuum limit is approached, with the area shrinking to zero. Including this point in Q_{44}^{elas} using its functional form poses no issue.

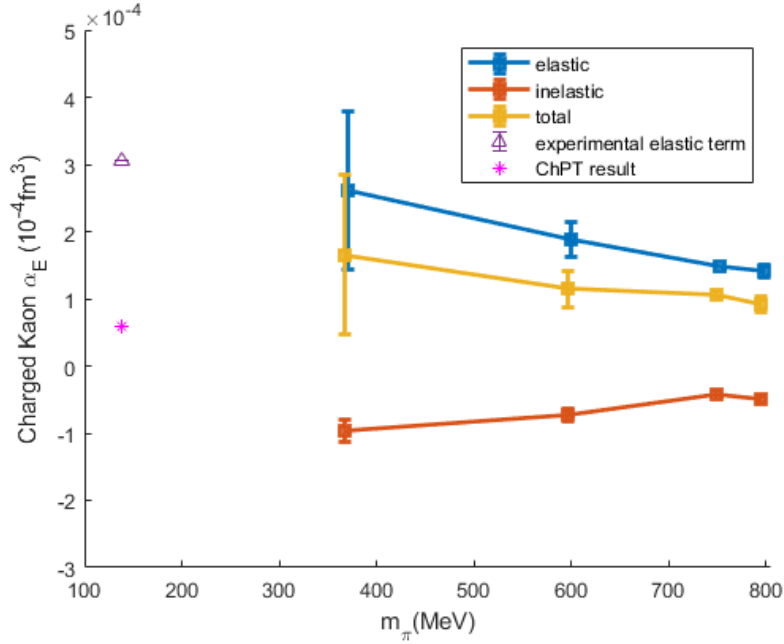


Figure 7: Kaon mass dependence of electric polarizability of a charged kaon from four-point functions in lattice QCD. Elastic and inelastic contributions correspond to the two terms in the formula in Eq.(1). Magenta triangle is the experimental PDG value for the elastic term. Pink star is the ChPT value for the kaon electric polarizability. The elastic data points are manually shifted to the right for better visibility.

The inelastic term is constructed by multiplying $2\alpha/q^2$ by the time integral; this entire term is a function of momentum. Since α_E is a static property, we smoothly extrapolate it to $q^2 = 0$. Due to the limitation of having only two momentum values, we use a linear fit for this extrapolation. Finally, we combine the two terms in the formula from Eq.(1) to calculate α_E in physical units.

To examine the trend at smaller pion masses, we will take the total values for α_E at four pion masses and perform a smooth extrapolation to the physical point. Currently, we only display a connected line between data points. The results are summarized in Fig. 7. At the pion masses studied, our lattice results reveal a distinct pattern for electric polarizability: the elastic term contributes positively, while the inelastic term contributes negatively but with a smaller magnitude. This partial cancellation results in a positive total value. The cancellation appears to persist as we approach the physical point, though it is less quantitatively conclusive, as indicated by the uncertainty bands from the extrapolations. This underscores the importance of investigating smaller pion masses in future simulations. The results in Fig. 7 show a similar trend to the results in Ref. [7] for the pion. It can be seen that the electric polarizability increases with decreasing pion mass. It also seems that an extrapolation to the physical point will result in a value higher than the ChPT result, which is what we see for the pion as well.

3.4 Conclusions

In this study, we have explored an alternative approach to calculating the electric polarizability of the charged kaon using four-point functions in lattice QCD. By leveraging four-point correlation

functions, we overcome challenges that arise from electro-quenching and the complexities of charged hadrons in external electromagnetic fields, as discussed in previous works [5, 6].

Our results highlight the separation of the elastic and inelastic contributions to the kaon's electric polarizability. The elastic term contributes positively, while the inelastic term introduces a smaller negative contribution, leading to a cancellation between the two terms. These findings are consistent with earlier studies of charged hadrons [9, 10].

The relatively small number of configurations (99) used in this study introduces statistical uncertainties. We are working towards using a larger configuration set (500) to help reduce these uncertainties significantly. Moreover, the current simulation utilizes quenched Wilson fermions, which have known limitations, as evidenced in earlier studies [3, 11]. Future work will involve using dynamical fermions, which will better reflect the physical quark content and improve the reliability of the results.

As we move forward, we will also be using data for 4 momenta instead of 2, and apply more sophisticated fitting methods, such as the z -expansion [8], to enhance the accuracy of our results. Our analysis also suggests that a more detailed exploration of smaller pion masses will be important for refining the extrapolation to the physical point, a task that has been undertaken in other works studying meson polarizabilities [2, 12].

Acknowledgments

We would like to acknowledge support from the Baylor College of Arts and Sciences Summer Research Award (SRA) program. This work was supported in part by DOE Grant No. DE-FG02-95ER40907. The authors acknowledge the Texas Advanced Computing Center (TACC) at The University of Texas at Austin for providing computational resources that have contributed to the research results reported within this paper.

References

- [1] H.R. Fiebig, W. Wilcox and R.M. Woloshyn, *A Study of Hadron Electric Polarizability in Quenched Lattice QCD*, *Nucl. Phys. B* **324** (1989) 47.
- [2] M. Lujan, A. Alexandru, W. Freeman and F.X. Lee, *Finite volume effects on the electric polarizability of neutral hadrons in lattice QCD*, *Phys. Rev.* **D94** (2016) 074506 [1606.07928].
- [3] W. Freeman, A. Alexandru, M. Lujan and F.X. Lee, *Sea quark contributions to the electric polarizability of hadrons*, *Phys. Rev.* **D 90** (2014) 054507 [1407.2687].
- [4] XQCD collaboration, *Towards the nucleon hadronic tensor from lattice QCD*, *Phys. Rev.* **D 101** (2020) 114503 [1906.05312].
- [5] M. Burkardt, J. Grandy and J. Negele, *Calculation and Interpretation of Hadron Correlation Functions in Lattice QCD*, *Annals Phys.* **238** (1995) 441 [hep-lat/9406009].
- [6] W. Wilcox, *Lattice charge overlap. 2: Aspects of charged pion polarizability*, *Annals Phys.* **255** (1997) 60 [hep-lat/9606019].

- [7] F.X. Lee, A. Alexandru, C. Culver and W. Wilcox, *Charged pion electric polarizability from four-point functions in lattice QCD*, *Phys. Rev. D* **108** (2023) 014512 [2301.05200].
- [8] G. Lee, J.R. Arrington and R.J. Hill, *Extraction of the proton radius from electron-proton scattering data*, *Phys. Rev. D* **92** (2015) 013013 [1505.01489].
- [9] M. Engelhardt, *Neutron electric polarizability from unquenched lattice QCD using the background field approach*, *Phys. Rev. D* **76** (2007) 114502 [0706.3919].
- [10] F.X. Lee, L. Zhou, W. Wilcox and J.C. Christensen, *Magnetic polarizability of hadrons from lattice QCD in the background field method*, *Phys. Rev. D* **73** (2006) 034503 [hep-lat/0509065].
- [11] A. Alexandru and F.X. Lee, *The Background field method on the lattice*, *PoS LATTICE2008* (2008) 145 [0810.2833].
- [12] R. Bignell, W. Kamleh and D. Leinweber, *Magnetic polarizability of the nucleon using a Laplacian mode projection*, *Phys. Rev. D* **101** (2020) 094502 [2002.07915].